

Flow Asymmetry in Symmetric Multiple Impinging Jets: A Large Eddy Simulation Approach

N. Kharoua and L. Khezzar*

Department of Mechanical Engineering, The Petroleum Institute, P.O. Box 2533, Abu Dhabi, United Arab Emirates

Received 16 April 2011; accepted 22 September 2011

الجريان غير المتناظر في النوافير الهوائية المتناظرة المتعددة الفوهات: منهج التمثيل العددي للدوامات الكبيرة
ن. خرواع ول. خزار*

الخلاصة: تم استخدام الطرق العددية لدراسة تدفق الهواء المنبعث من فوهات دائرية مصفوفة بالتوازي والمنصب على صفيحة مستوية ومسخنة. ولتوضيح التفاصيل الدقيقة للتدفق اللحظي والمتوسط فقد تم استعمال النموذج الرياضي المسمى بنموذج محاكاة الدوامات الكبيرة ذات التدفق المضطرب تحت ظروف تدفق متمثلة برقم رينولدز يساوي 20000 والمحسوب على أساس قطر فوهة التدفق. بالإضافة إلى ما هو معلوم عن التدفق من فوهة واحدة فإن التفاعل بين التدفقات من الفوهات المتجاورة قد تم توضيحه بنجاح. وللتوفير في استهلاك وقت الحاسوب فقد تم تقليل الحيز المدروس إلى الربع وذلك بالاستفادة من التناظر الموجود. وأسفرت الدراسة عن التثبت من عدم التناظر في سرعة الجريان والذي سبقت ملاحظته في الدراسات النظرية والمخبرية السابقة. ومع بعض الفروق البسيطة قرب سطوح التناظر فقد بين النموذج الرياضي المستعمل البصمات البيضاوية لانتقال الحرارة (من خلال رقم نيوست) والتي سبق ولوحظت مخبريا. كما تم تأكيد النتائج المخبرية والحسابية حول اللاتناظر الموجود في المستويات الأفقية والموازية والقريبة من الصفيحة المسخنة. كذلك تم التوصل إلى معرفه طبيعة منطقة الحركة الدوامية المسؤولة عن عدم التناظر في الجريان والمعروف حصولها نتيجة التفاعل بين التدفقات من الفوهات المتجاورة، حيث شوهد حصول هذه الحركة فقط في جانب واحد من الخط القطري ما بين الفوهة المركزية وأبعد فوهة.

المفردات المفتاحية: النوافير الهوائية المتعددة الفوهات، التمثيل العددي للدوامات الكبيرة، انتقال الحرارة، الجريان المضطرب

Abstract: A numerical study on in-line arrays of multiple turbulent round impinging jets on a flat heated plate was conducted. The Large Eddy Simulation turbulence model was used to capture details of the instantaneous and mean flow fields. The Reynolds number, based on the jets diameter, was equal to 20,000. In addition to flow features known from single jets, the interaction between the neighboring jets was successfully elucidated. Symmetry boundary conditions were imposed to reduce the computational domain to only a quarter. In accordance with previous numerical and experimental works, the asymmetry in the velocity field near to the impingement plate was also found to exist. LES showed oval imprints of the Nusselt number similar to experiments but with some discrepancies on the symmetry boundaries. The asymmetry, observed in previous experimental and numerical results, in the horizontal planes, parallel and close to the impingement wall, was confirmed. The recirculation zone responsible for asymmetry, known to develop due to the wall jets interaction, was seen in only one side of the diagonal formed by the central and the farthest jets.

Keywords: Multiple impinging jets, Large eddy simulation, Heat transfer, Turbulence

1. Introduction

The present paper reports on Large Eddy simulation (LES) of multiple turbulent round impinging jets on a heated flat plate. Because of the high heat transfer rates that can be achieved using them, impinging jets

are employed in a wide range of important industrial applications for cooling, heating, and drying solid obstacles or paper and textiles with different shapes, cooling of electronics components, and annealing of steel.

*Corresponding author's e-mail: lkhezzar@pi.ac.ae

Single impinging jets have been extensively studied (Yokobori *et al.* 1977; Hadžiabdic and Hanjalic 2008) and the turbulent flow and the heat transfer they induce are well elucidated. Nonetheless some features are still being investigated such as the Nusselt number dip and second peak observed for small jet-slot-to-impingement distances. The parameters affecting single impinging jets flow behaviour are: the Reynolds number, the slot shape, the slot-to-impingement distance, and the impingement obstacle shape. The Multiple impinging jets represent an extension of the single jet where more complex phenomena take place. The interaction of the jets generates secondary flows in the space separating the jets depending on their distribution and pitch in addition to the other parameters mentioned for the single jet case. Impinging jets create also horizontal wall jets along the impingement surface which , impact at a certain distance from the impingement region. The impact causes the wall jets to deviate in an uplift motion then to be entrained downward by the free jets. Thus, recirculation zones are created in the corners formed by the free and the wall jets. Garimella and Schoeder (2001) have studied the local heat transfer distributions for three different configurations of in-line jet arrays compared with a single jet. They noticed that the central jet in the nine-jet array generated a higher heat transfer coefficient at the stagnation point in comparison with the single jet at the same Reynold number. Thielens *et al.* (2003) have conducted a simulation work on in-line and circular impinging jets using the $k-\varepsilon$ and v^2-f turbulence models and latter on using a modified second-moment-closure model (Thielen *et al.* 2005). They have considered a quarter of the real domain relying on symmetry boundary conditions. Their results showed, surprisingly for the in-line jets configuration, an asymmetry of the flow along the diagonal axis. Geers *et al.* (2006), in their experimental work, have confirmed the existence of the asymmetry noticed in Thielen's works thereby demonstrating that it was not a CFD artifact. In addition they have studied a hexagonal configuration of multiple jets with sharp-edged and contoured jet-outlet-orifices. The Reynolds averaged Navier-Stokes (RANS) equations and corresponding turbulence models are still being used due to their reasonable computational-tools requirements. Xing *et al.* (2010) have compared the performance of in-line and staggered jets under the effect of variable cross-flow regimes. They used the Shear Stress Transport (SST $k-\omega$) turbulence model (Menter 1994). They found that the in-inline configuration yielded better heat transfer rates. The SST $k-\omega$ appears to be the best RANS model for predicting multiple jets flows as stated by Spring *et al.* (2010). Indeed, they used it to investigate the heat transfer occurring during the

process of cooling combustor liner heat shield. The slots were irregularly distributed. They noticed that the numerical simulation over-predicted the Nusselt number at the impingement point by up to 100% with an average error of 40%.

Large eddy simulation allows the resolution of large energetic scales of motions whereas the small dissipative scales are modeled through a sub grid model. It thus captures more flow details compared to the classical RANS models and offers a viable alternative for computing industrial flows between RANS on the one hand and direct numerical simulations (DNS) which require intensive resources on the other. To the authors knowledge no LES predictions for this type of flow have been reported before. In the present work the LES turbulence model is used to predict the turbulent flow and heat transfer features of in-line multiple round impinging jets to find out if the flow asymmetry is still present and discuss the correlation between flow and heat transfer from instantaneous flow properties. It is seen that LES captures the interaction between the adjacent jets and their effects on heat transfer with very good accuracy. The numerical results obtained are validated based on the detailed experimental work of Geers *et al.* (2006).

2. Geometry and Computational Grid

The configuration studied corresponds to the in-line arrays of jets of the experimental work done by Geers *et al.* (2006). The geometry and relevant dimensions and orientation are shown in Fig. 1. Each jet nozzle has a diameter $D = 13$ mm. The nozzles-to-impingement distance H and the pitch S are both equal to $4D$. Based on an inlet velocity of 23.88 m/s and air properties at room temperature, the Reynolds number for each jet is 20,000. A multi-bloc hexahedral mesh of about 9.5 million computational cells was generated (Fig. 2). Only one quarter of the domain has been considered in the present simulation work relying on symmetric boundary conditions. Thus, only four among the nine jet nozzles located on a solid plate are represented in Fig. 2. The mesh was refined in the regions where high gradients were expected which are, the free-shear layer developing from the orifice contour and the wall jet layers near the two walls.

The non dimensional distance y^+ was inferior to 1.8 on the lower wall and to 7 in the upper wall.

3. Equations and Solution Methods

3.1 Mathematical Formulation

The fluid is assumed incompressible and the filtered continuity and momentum equations solved are given by:

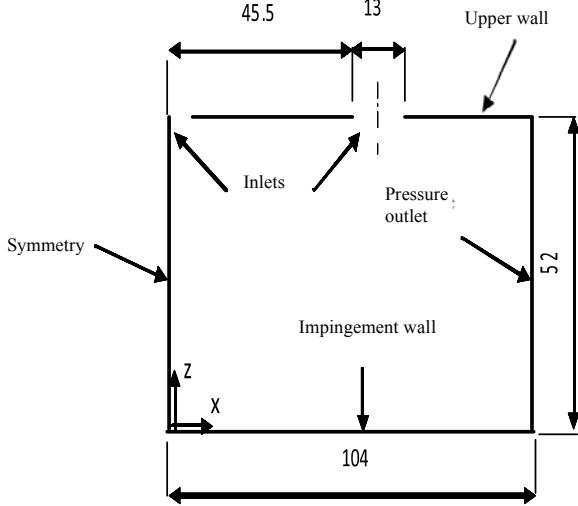


Figure 1. Geometry and boundary conditions, dimensions in mm

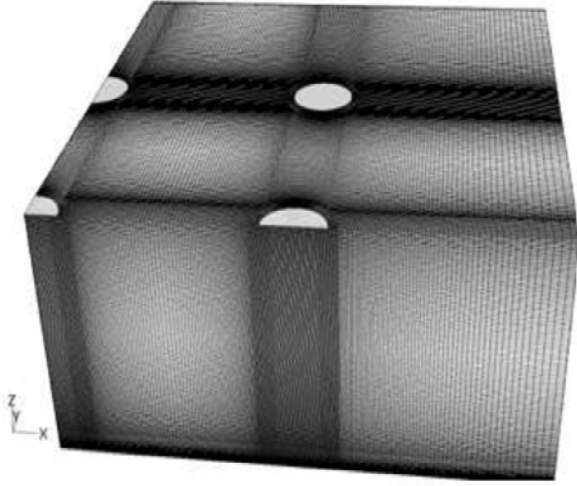


Figure 2. Computational mesh

$$\frac{\partial \bar{u}}{\partial x} = 0 \quad (1)$$

$$\frac{\partial(\rho \bar{u})}{\partial t} + \frac{\partial(\rho \bar{u} \bar{u})}{\partial x} = \frac{\partial \sigma}{\partial x} - \frac{\partial \bar{p}}{\partial x} - \frac{\partial \tau}{\partial x} \quad (2)$$

where the variables with an over bar represent the filtered (the locally averaged) values. The laminar stress tensor is given by:

$$\sigma = \mu \left(\frac{\partial \bar{u}}{\partial x} + \frac{\partial \bar{u}}{\partial x} \right) \quad (3)$$

The subgrid stress accounting for the unresolved scales contribution is defined by:

$$\tau = \rho (\overline{uu} - \bar{u}\bar{u}) \quad (4)$$

It is modeled using the Boussinesq hypothesis

$$\tau - \frac{1}{3} \tau \delta = 2\mu \bar{S} \quad (5)$$

where

$$\bar{S} = \frac{1}{2} \left(\frac{\partial \bar{u}}{\partial x} + \frac{\partial \bar{u}}{\partial x} \right) \quad (6)$$

The Smagorinsky-Lilly subgrid scale turbulent eddy-viscosity is obtained from

$$\mu = \rho L \sqrt{2\bar{S}} \quad (7)$$

L_S in Fluent, is calculated using

$$L = \min(\kappa d, CV) \quad (8)$$

where κ is the Von Karman constant, d is the closest distance to the wall, C_S is the Smagorinsky constant dynamically calculated based on the information included in the resolved scales of motion (Germano *et al.* 1991; Lilly 1992) and V is the volume of the computational cell.

The energy equation is written as:

$$\frac{\partial \bar{T}}{\partial t} + \bar{u} \frac{\partial \bar{T}}{\partial x} = \frac{\partial}{\partial x} \left(\frac{\nu}{\sigma} \frac{\partial \bar{T}}{\partial x} \right) + \frac{\partial q}{\partial x} \quad (9)$$

where σ is the Prandtl number and the subgrid-scale temperature flux is defined as

$$q = \bar{u}\bar{T} - \bar{u}T \quad (10)$$

and is calculated using the subgrid scale turbulent Prandtl number under a gradient hypothesis

$$q = \frac{\nu}{\sigma} \frac{\partial \bar{T}}{\partial x} \quad (11)$$

The turbulent Prandtl number is estimated by applying the dynamic procedure to the subgrid-scale flux (see Germano *et al.* 1991, Lilly 1992).

3.2 Boundary Conditions, Discretization, and Simulation Strategy

Figure 1 illustrates the boundary conditions used. Uniform velocity profiles were imposed at the inlet with a turbulence intensity of 0.8%. The fluctuating velocities were generated using the spectral synthesizer (Kraichnan 1970, Smirnov *et al.* 2001). The temperature at the inlet was set to 299 K. No slip condition was used for the upper wall with a constant temperature equal to that of the inlet. At the impingement wall, no slip condition was imposed in conjunction with a constant heat flux of 1562.5 W/m^2 . For the out-

lets, zero relative pressure boundary condition was employed and a low turbulence intensity of 0.1%. The temperature of the surroundings, at the outlets, was similar to that of the inlets.

The standard scheme was used for the pressure interpolation while a bounded central differencing scheme was used to discretize the convective term in the filtered Navier-Stokes and energy equations.

A steady mean flow was computed using the Reynolds stress turbulence model to provide reasonable initial conditions for the LES simulation. Subsequently, an LES simulation was conducted during around 0.054 s corresponding to few times the residence time of the flow based on a flow average velocity. When the flow stabilized, the statistics were collected over a time interval corresponding to 1.5 times the characteristic residence time.

The local time-averaged Nusselt number is calculated using

$$\overline{Nu}(x, y) = \frac{1}{N} \sum (x, y, t) \quad (12)$$

where $Nu(x, y, t)$ is the local and instantaneous Nusselt number at a position (x, y) along the impingement wall at time t , based on the slot diameter D and the difference between the reference (slot jet) temperature and the wall temperature and N is the number of samples taken for the calculation of the mean Nu . The calculations were performed with fluent code running in parallel mode using 16 processors.

4. Results and Discussions

The first part of this section represents a validation of the mean field by comparison with the experimental results of (Geers *et al.* 2006). The second one illustrates some features of the flow and its effects on the heat transfer.

4.1 Validation of the Mean Field

The Nusselt number reflects the heat transfer strength. Figure 3 shows, relatively, a good agreement between the results obtained using LES and the experiments. Peaks of the Nusselt number Nu deviate slightly from the positions of the inlet centers. The imprint is oval although the inlets are circular. It has been explained in (Geers *et al.* 2006) by the effect of the wall jets, generated after the impingement of the free jets on the flat surface and acting as a cross flow, on the surroundings deviating the neighbor impinging jets. Figure 4, by superimposing mean z velocity and streamlines on the symmetry plane $x/D=0$, illustrates the explanation of the aforementioned deviation of Nu imprints. The experiments show that the surrounding air is entrained from the top close to the central jet whereas the LES captures a different behaviour. Two

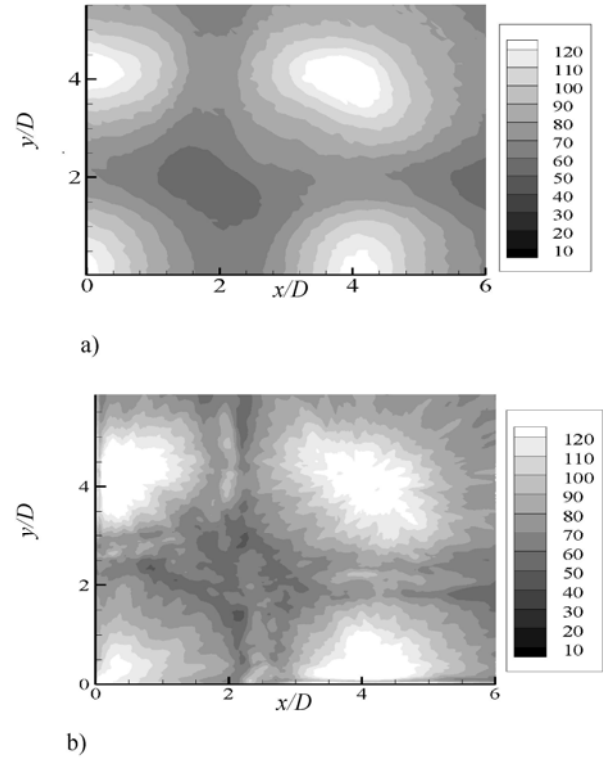


Figure 3. Average Nusselt number on the impingement wall: a) Experiments, b) LES

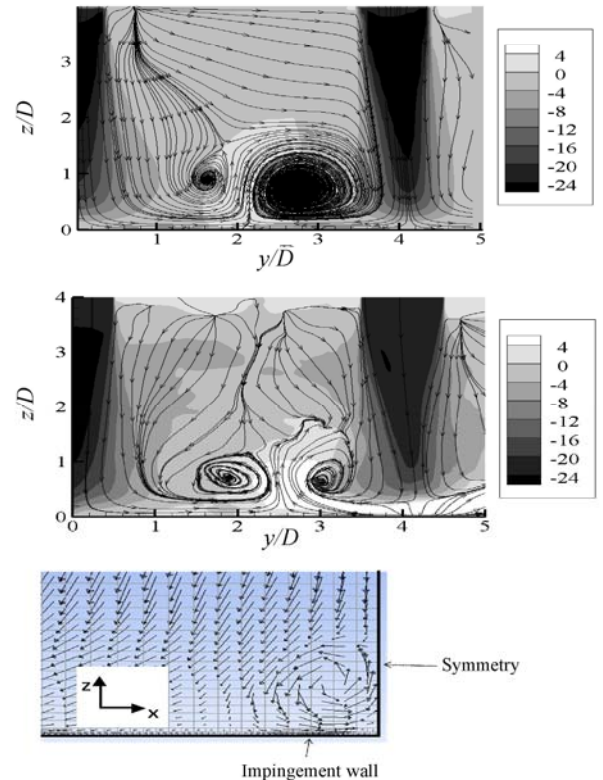


Figure 4. Mean z velocity and streamlines superimposed on the plane $x/D=0$: a) Experiments, b) LES, c) velocity vectors near the corner formed by the impingement wall and the symmetry plane

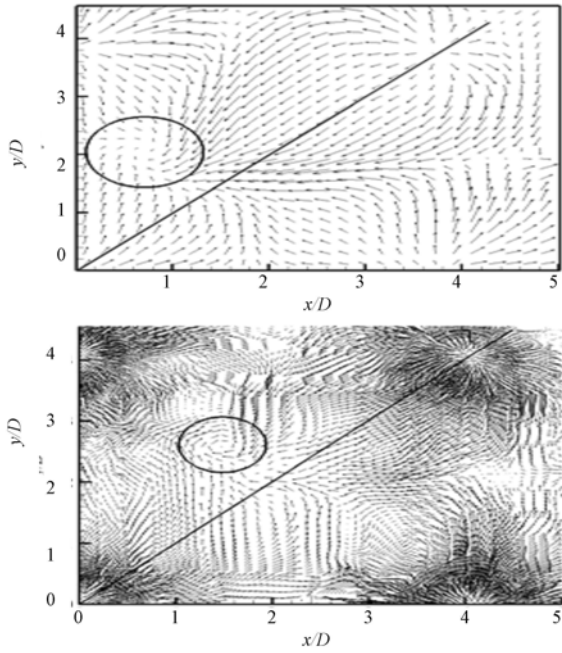


Figure 5. Mean-velocity vectors on the horizontal plane $z/D=0.54$: a) Experiments, b) LES

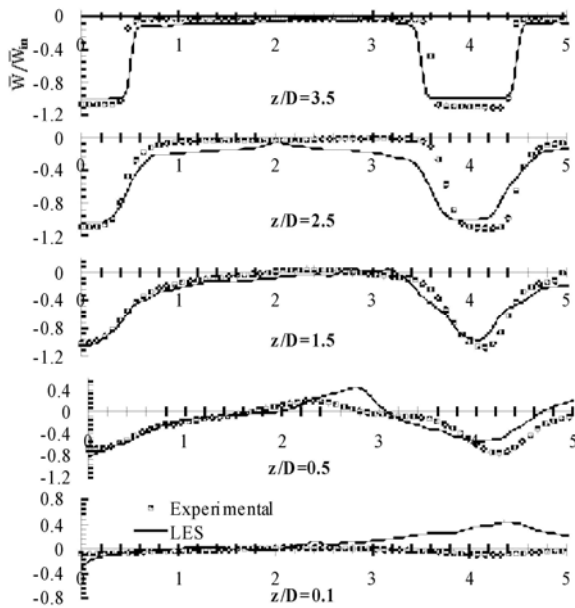


Figure 6. Mean z velocity profiles in the y direction on the plane $x/D=0$ at different positions z/D

counter-rotating vortices are generated after the wall jets impact in the space separating the two jets (Thielen *et al.* 2005) reported that only a modified Reynolds stress turbulence model could detect such behaviour.

At $y/D=4$, the simulation results show an ascending flow just at the impingement region while it should be descending. Investigating this strange behaviour, it has been found that a clockwise recirculation zone

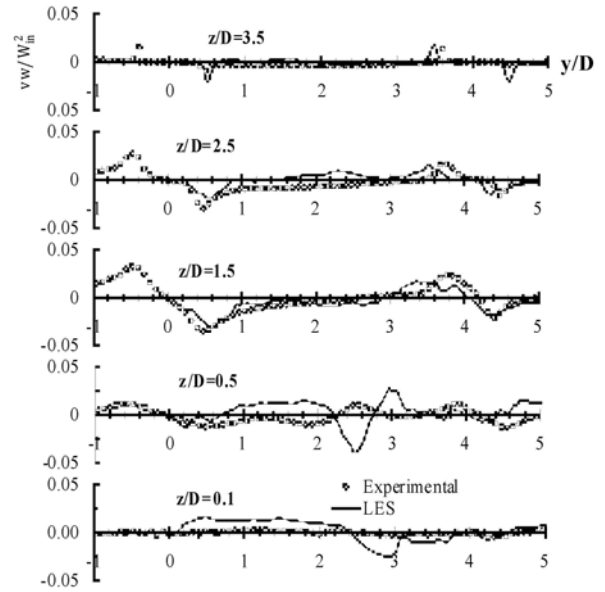


Figure 7. Reynolds shear stress vw profiles in the plane yz at $x/D=0$

developed in the perpendicular plane $y/D=4$ in that region. This phenomenon, not present in the experiments, might be due to the symmetry boundary condition used at $x/D=0$.

Mean-velocity vectors, plotted on an horizontal plane at $z/D=0.54$, are depicted in Fig. 5. The asymmetry mentioned by (Thielen *et al.* 2005, Geers *et al.* 2006) is detected in the present work. A vortex appears in only one side of the diagonal although at a different location than the experiments. Geers *et al.* (2006) explained that the vortex location could change from one side of the diagonal to the other instantaneously but in around 70% of the snapshots, it was found to have a preferred position. No reason for this preference was given.

Profiles of the mean z velocity, normalized by the inlet velocity at the jet centerline, are shown in Fig. 6 at different horizontal positions along the y axis on the plane $x/D=0$.

Very good agreement between the experimental and simulation results is observed. The anomaly at $z/D=0.1$ and $y/D=4$ ie closest to the wall has been explained previously by the possible effect of the symmetry boundary condition. It can be seen that the central jet ($y/D=0$) is enlarged when moving towards the impingement wall while the neighbouring-jet cross-section diminishes deviating outward from the center at $y/D=4$.

Figure 7 depicts profiles of the Reynolds shear stress vw in the plane yz at $x/D=0$. The profiles plotted at $z/D=1.5$ and higher horizontal positions show a very good prediction of the shear stress by LES compared

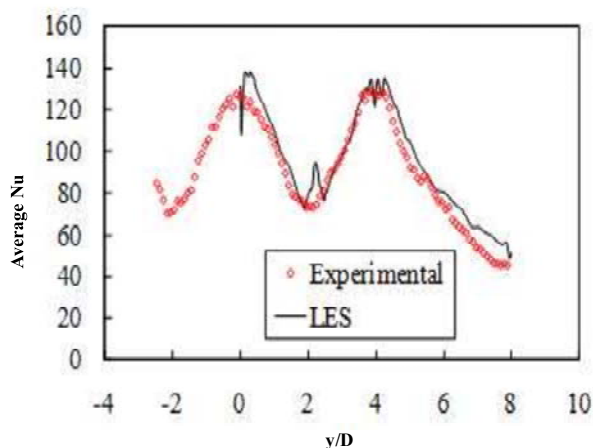


Figure 8. Profiles of the Nusselt number on the intersection line between the symmetry plane $x/D=0$ and the impingement wall

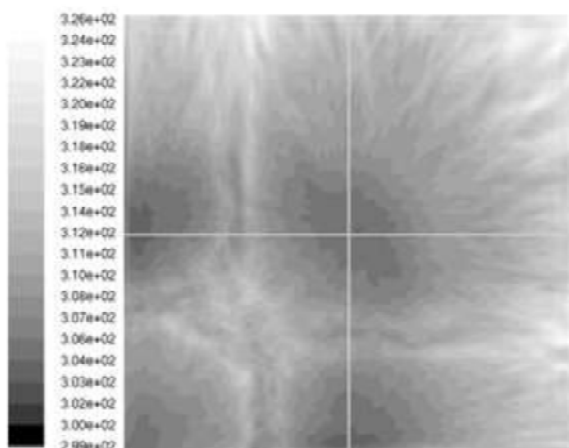


Figure 9. Contours of the mean temperature on the impingement wall (K)

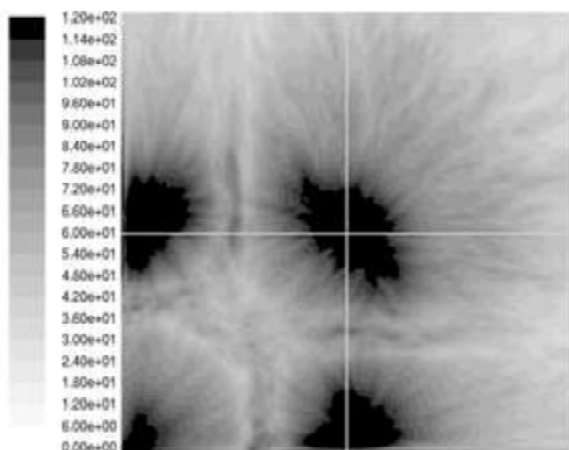


Figure 10. Contours of the average Nusselt number on the impingement wall

with experimental results. Close to the impingement wall, at $z/D=0.1$ and $z/D=0.5$, the profiles deviate remarkably. In fact, the symmetry boundary condition used remains valid at high positions where no significant jet flapping or jet-jet interaction occur. Close to

the impingement wall, the main discrepancies are observed in the inter-space separating the jets.

A quantitative validation of the Nusselt number distribution is illustrated in Fig. 8. The profile plotted in the symmetry plane at $x/D=0$ shows a good agreement between LES and the experimental results. Whereas, it was found in previous simulation works (Xing *et al.* 2010, Spring *et al.* 2010) that the RANS turbulence models overestimate the Nusselt number peaks with an average of 40%. In the inter-space, separating the individual jets, a small amplitude peak can also be observed. This however was not observed in the experiments where liquid crystal thermography was used most probably because of the spatial resolution of the technique. This region corresponds to the impact of the wall jets resulting from the deviated jets after impinging on the heated wall and, hence, is highly unstable and consequently a local enhancement of the heat transfer nearby is most probable.

4.2 Effect of the Flow Field on the Heat Transfer

To investigate the effect of the flow on the heat transfer contours of the mean pressure, the turbulent kinetic energy, the mean temperature, and the average Nu are plotted on or close to the impingement wall in Figs. 9-12. Figures 9 and 10 show that the mean temperature and the average Nu have identical imprints since the Nu is proportionally dependent on the temperature.

In Fig. 11, the imprint of the mean pressure contours, resulting from the forces exerted by the jet flow on the impingement wall, appears to have a similar shape to that of the average Nu . Indeed, oval imprints of the surrounding jets are deviated from the inlet centres showed by the intersecting lines. The same remark can be done for the turbulent kinetic energy (Fig. 12) plotted on the plane constituted from the closest nodes to the impingement wall. The ovality of the imprints, corresponding to high-level turbulence, is clear.

Figures 13 and 14 illustrate the interaction of the dynamic field with the heat transfer. In Fig. 13, profiles of the instantaneous Nusselt number and the friction coefficient along the intersection line between the symmetry plane ($x/D=0$) and the impingement wall are shown. At the impingement regions ($y/D=0$ and $y/D=4$), it can be seen that the well-known Reynolds analogy is not valid where Nu maxima coincide with friction coefficient minima. Hadžiabdic and Hanjalic (2008) have reported similar results for a single round jet. They related the high peaks of the Nusselt number and the friction coefficient, around and far from the impingement point, to the impact of the large-scale eddy structures which, according to them, play a key role in heat transfer.

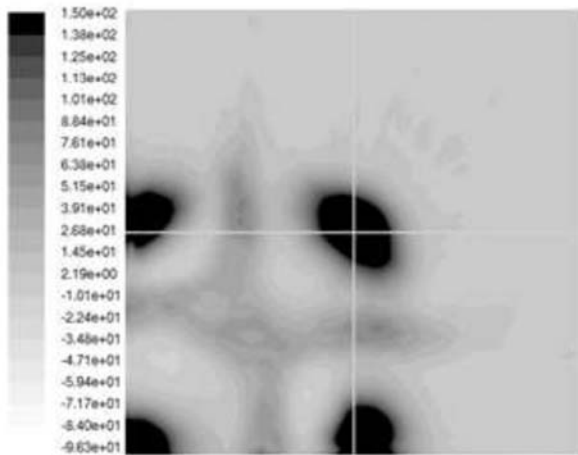


Figure 11. Contours of the mean static pressure on the impingement wall (Pa)

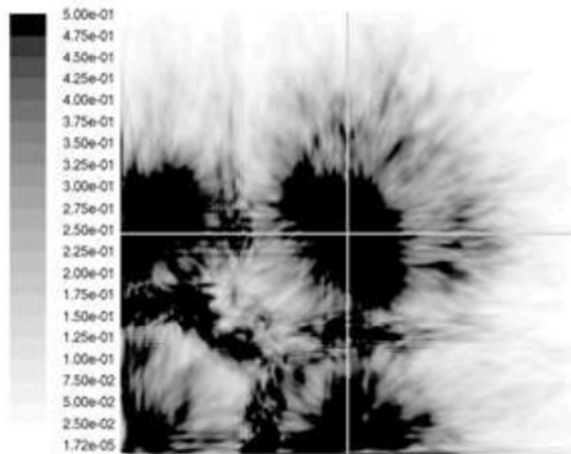


Figure 12. Contours of the turbulent kinetic energy on the plane corresponding to the closest nodes to the impingement wall (m^2/s^2)

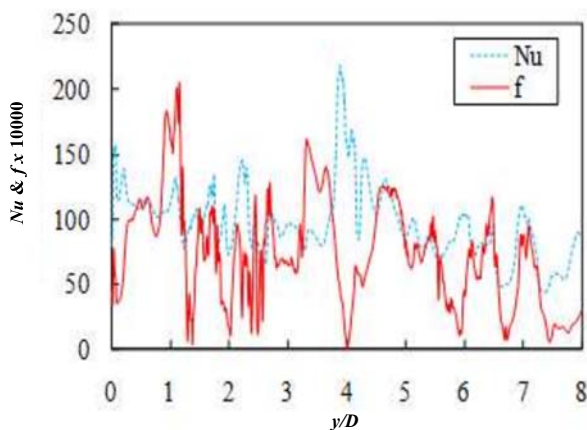


Figure 13. Profiles of the Nusselt number and the friction coefficient on the intersection line between the symmetry plane $x/D=0$ and the impingement wall

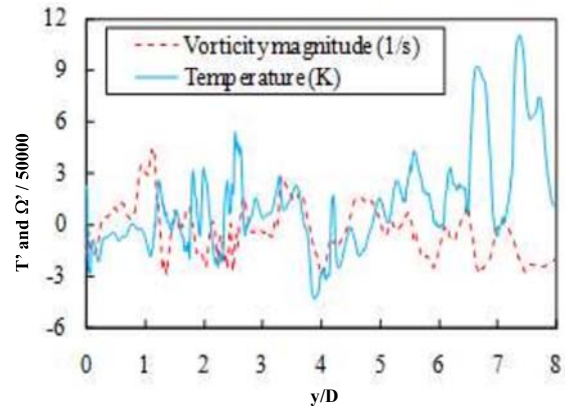


Figure 14. Profiles of vorticity magnitude and instantaneous temperature on the intersection line between the symmetry plane $x/D=0$ and the impingement wall

In the same manner, Fig. 14 shows profiles of vorticity magnitude superimposed with profiles of instantaneous temperature. It can be seen that high vorticity corresponds to low temperatures. This confirms, somehow, the statement that large turbulent structures affect strongly the heat transfer.

Finally, 3D contours of the mean z velocity showing the potential core of the four jets are illustrated in Fig. 15. Figure 15a shows a flow acceleration for the central jet (see also simulation results in Fig. 4) which doesn't exist in the neighbouring one probably due to the fact that the central jet undergoes a choking-like effect from the surrounding jets. The neighbouring jet is clearly deviated from its axis. It is also the case for the jet placed at an angle of 45° (see Figure 15 b) deviating along the diagonal perpendicular to that passing by the origin $(0,0)$. In Figure 15c, it can be seen that the jet placed at 45° is symmetric taking as reference the diagonal passing by the origin).

Conclusions

Large eddy simulation (LES) using the Smagorinsky dynamic sub-grid scale model was used to simulate the flow and heat transfer behaviour of multiple in-line jets impinging on a heated flat plate.

The simulation results were in good agreement with experimental results although some discrepancies have been noticed due, probably, to the symmetry boundary conditions used. Despite the symmetry of the geometry, a complex asymmetric flow pattern was observed and well captured in accordance with previous studies.

Contours of the mean pressure, the turbulent kinetic energy, the mean temperature, and the average Nusselt number showed a strong dependence of the heat transfer on the flow field structure. Different behaviour has been observed for the central and the

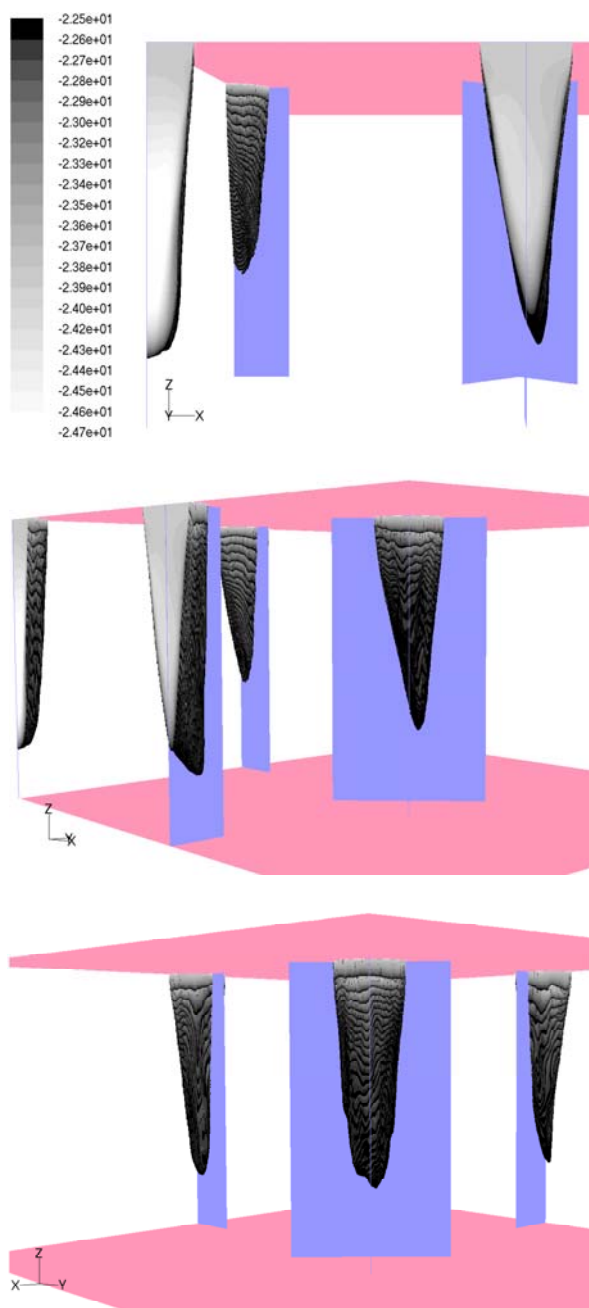


Figure 15. 3D contours of the mean z velocity (the vertical planes corresponding to the inlets symmetry planes)

outer jets. The neighboring jets deviate outward under the effect of the central jet which causes the Nusselt peaks to deviate from the geometrical axis of the slots.

The use of symmetry boundary conditions, for such flows, has been found realistic far from the impingement wall where the mean and the turbulent flow features were accurately captured. Close to the boundary where symmetry was imposed, acting as a wall, the jet flapping was artificially suppressed. This led to the generation of recirculation zones in the corner formed

by the impingement wall and the symmetry boundary. The recirculation zones acted as an obstacle to the free jets preventing them from directly impinging on the flat plate resulting in somewhat unrealistic behaviour of the flow and heat transfer close to the impingement region.

Acknowledgments

Financial support to Dr N. Kharoua from the Petroleum Institute is gratefully acknowledged.

References

- Garimella SV, Schroeder VP (2001), Local heat transfer distributions in confined multiple air jet impingement. *ASME Journal of Electronic Packaging* 123(3):165-172.
- Geers L, Hanjalic K, Tummers M (2006), Wall imprints of turbulent structure and heat transfer in multiple impinging jet arrays. *J. Fluid Mech.* 546:255-284.
- Germano M, Piomelli U, Moin P, Cabot WH (1991), A dynamic subgrid-scale eddy viscosity model. *Physics of Fluids* 3:1760-1765.
- Hadziabdic M, Hanjalic K (2008), Vortical structures and heat transfer in a round impinging jet. *J. Fluid Mech.* 596:221-260.
- Kraichnan R (1970), Diffusion by a random velocity field. *Physics of Fluids* 11:21-31.
- Lilly DK (1992), A proposed modification of the germano subgrid-scale closure model. *Physics of Fluids* 4:633-635.
- Menter FR (1994), Two-equation eddy-viscosity turbulence models for engineering applications. *AIAA Journal* 32:69-289.
- Smirnov R, Shi S, Celik I (2001), Random flow generation technique for large eddy simulations and particle-dynamics modeling. *J. Fluids Eng.* 123:359-371.
- Spring S, Lauffer D, Weigand B, Hase M (2010), Experimental and numerical investigation of impingement cooling in a combustor liner heat shield. *ASME J. Turbomach* 132:011003.
- Thielen L, Hanjalic K, Jonker H, Manceau R (2005), Predictions of flow and heat transfer in multiple impinging jets with an elliptic-blending second-moment closure. *Int. J. Heat and Mass Transfer* 48(8):1583-1598.
- Thielen L, Jonker H, Hanjalic K (2003), Symmetry breaking of flow and heat transfer in multiple impinging jets. *Int. J. Heat Fluid Flow* 24(4): 444-453.
- Xing Y, Spring S, Weigand B (2010), Experimental

and numerical investigation of heat transfer characteristics of inline and staggered arrays of impinging jets. *J. heat transfer* 132:092201.
Yokobori S, Kasagi N, Hirata M (1977),
Characteristic behaviour of turbulence in the stag-

nation region of a two-dimensional submerged jet impinging normally on a flat plate. *First Int. Symp. Turbulent Shear Flows*, University Park, Penn, USA.